Experimental and numerical analysis of Novel 9 DOF Robotic Manipulator for Computed Tomography Guided Medical Procedure

Shubham Kamlesh Shah[a], Ruby Mishra*[b]

[a,b] School of mechanical engineering, KIIT deemed to be University, Bhubaneswar-751024, India
[a]e-mail: shubham.prasad1@gmail.com, Mob. No.: +91-9861501763
[*b]e-mail: rubymishrafme@kiit.ac.in, Mob.No.: +91-9437678405

Abstract:

One of the most common procedures implemented in the diagnosis of cancer and tumour is percutaneous biopsy under computed tomography (CT) image guidance. A 9-DOF hybrid redundant fully actuated robotic manipulator with a novel arc and train design is developed the retrieval of suspected tissue for biopsy procedure under CT guidance. The mathematical model of the robotic manipulator is formulated using standard DH convention. Inverse kinematics of the novel arc and train structure for CT bed mountability is also derived in this research. 3D-CAD model of the robot is developed and compared with the CT machine and a human model in SolidWorks 201 simulation is performed using MATLAB.A dual camera system and the actuator's internal position sensors are used to obtain and plot the robot's deviation analysis from the goal during experimentation. Actuator sensor data is plotted against the required profile in order to determine the causes of the deviation and assess the positional trajectory and velocity trajectory profile. The deviations in position in the range of 3 to 3.5 mm in each of X, Y, or Z axes and the variance in the angle is between 0.4 and 0.55 degrees. It performed amicably under simulated laboratory conditions.

Keywords: *9-DOF redundant robotic manipulator; Theoretical Simulation; Experimental validation; Deviation analysis; Image processing; CT image guidance.*

1. Introduction

Robotics is a field of technology that has changed the world in multiple ways. Production in industries has been revolutionized by implementing robotics on a larger scale than ever before. Surgical robots are being used in top-level medical institutions around the world. Robots have also helped patients in post-operative rehabilitation under physiotherapy. Before treatment, diagnosis is required. In these papers, a robotic manipulator was created with CT scan images as a guide in order to execute a biopsy. The CT scan images can be used as input for the robotic manipulator in order to identify the coordinates and angle of the biopsy needle's point of entry. [1,2]

Tissue retrieval procedure using computed tomography (CT) image guidance has become one of the common practices for the biopsy procedure. When a medical doctor suspects cancerous or tumorous growth inside a patient using a CT image, it warrants further pathological findings to determine the type of cancer or tumour. The process of a pathological finding of such suspected tissue is known as a biopsy procedure. Conducting a biopsy procedure requires tissue samples. These suspected abnormal tissue samples are retrieved using a CT image as a reference for its position. There is opportunity for improvement even if the manual freehand approach is used globally with appropriate precision. Human limitations such as hand tremor and less experience are some of the major hurdles in the tissue retrieval method [3]. Here, a strategy was put forth for using the CNN network to separate the liver from the abdomen's computed tomography (CT) picture and for training a novel technique for discovering and classifying liver lesion pre-histological results using CNN's multi-channel deep learning (MDL-CNN) [4.-5]. To eliminate these hurdles during tissue retrieval under CT guidance, a novel robotic system is developed in this research.

A Survey of robotic and non-robotic systems designed for the improvement of percutaneous tissue retrieval procedure is performed. There are needle tracking systems and direct needle manipulation systems, which provide data in real-time for tracking the needle in the graphical form concerning the target coordinates for the process of tissue retrieval. There are three types of needle tracking systems: optical, electromagnetic, EM and mechanical, based on the functioning principle. Some examples of optical tracking system include Micron Tracker, NDI Polaris [6] and clarion [7]. Many optical tracking systems are also available commercially, e.g. the pathfinder [8, 9], Medtronic [10], elite Navigation system, the stryker [11] and the CASination CAS-ONE [12]. ActiViews CT-guide [13, 14] are some of the optical tracking systems specifically designed for tracking biopsy needles during a biopsy procedure. Some examples of EM needle tracking systems are NDI Aurora [6] and Medtronic AxiEM [15]. The major drawback of the EM needle tracking system is the proximity of metallic objects. Some examples of mechanical needle tracking systems are the Phillip pinpoint system [16-19] and the

MicroScribe-G2X mechanical arm with 5-DOF [20]. The drawback of a mechanical needle tracking system is that the intervention process is manual and the medical doctor has to perform the procedure.

There are two types of direct needle manipulation systems, patient mounted and CT bed mounted. A needle guidance system is physically placed on the patient for the orientation of the biopsy needle. The needle is inserted manually after the correct orientation is achieved. Commercially available patient-mounted robotic devices include NeoRad Simplify [21, 22] and apriomed seestar [23, 24]. A Robopsy system is a stepper-actuated patient-mounted system developed at MIT [25, 15]. Two stepper motors orient the needle at the first target point for insertion. The other two stepper motors clamp and release the needle for insertion. The sterility of the patient could be compromised using a patient mounted system. Robots designed to guide a biopsy needle and retrieve tissue percutaneously while being mounted on a CT bed are known as CT bed-mounted systems. A CT bed mounted system called CT guide is developed by Bard [26-28]. This robot comprises a guide parallel to the CT bed attached to an arc-shaped arm, which can rotate about the guide as well. Another table-mounted system with a five DOF over bridge structure is named AcuBot [29, 30]. The actuation of Acubot is also mechanical and the joints are locked once the desired position is reached. Maarten Menno Arnolli designed and developed one of the latest robotic systems for biopsy procedures in 2017. This robotic manipulator is mounted on the CT bed and can position the needle after the CT image is taken. The insertion of the needle using this system is manual [31]. Diagnosis of COVID-19 using deep learning based on convolutional neural networks to segment and classify lung CT images [32]. The main aim of this research work is to design and fabricate a setup that can precisely control the speed and depth of needle insertion procedure Depth and velocity of insertion of needle in the linear actuator is controlled automatically with the help of rotary encoder. The automated control system is controlled with the help of MyRIO controller [33]. This research presents a tele operational five degrees of freedom (DOF) articulated industrial robotic arm with manual motion control based on remote vision [34-35]. The multi-objective optimal design of a brand-new 6-degree of freedom (DOF) hybrid spray-painting robot is the subject of this research [36]. By splitting it into serial and parallel components, its kinematic model may be determined. The virtual work idea is used to formulate the dynamic equation. In order to accurately construct the industrial feed forward controller and account for the robot's externally unknown dynamic load, the study suggests an iterative learning strategy. The presentation of a full linear feed forward controller is based on a common dynamic model. The Moore-Penrose Inverse and the PID learning rate are combined to provide an iterative design technique for iteratively updating the feed-forward controller [37] An overview of the work that has already been done on dynamic parameter identification of serial and parallel robots is provided. We list the techniques for estimating the dynamic parameters and evaluate the benefits and drawbacks of each technique. Both the trajectory optimization and the to-be-identified model are examined [38]. This study compares a Laser Navigation System (LNS-group) to a conventional approach to analyze the radiation dose and speed of needle interventions [39]. Here, when using a robotic IR assistance platform to replicate CT-guided biopsy and percutaneous ablation, improved needle accuracy and optimized probe geometry were seen. When accuracy could affect the outcome, such as in clinical CT-guided biopsy and RFA, this technology may be helpful [40]. In this paper, the technology, which permits accurate needle placement in a single insertion, was prepared for its initial clinical deployment [41].

From the literature survey, it is observed that none of the systems provides a breakthrough that can decimate direct human intervention while keeping the human factor at play. All the previous CT guided systems are patient-mounted or require manual intervention. This will increase the X-ray exposure of the patients and medical staff. Hence, there is a need for a fully automated accurate robotic manipulator. The robotic manipulator must have redundant DOF for obstacle avoidance and superior dexterity within the constrained workspace of the CT bore a.k.a. CT scanning area.

Hence, the primary objective of this research is to develop an automated and fully actuated redundant robotic manipulator for CT image-guided tissue retrieval medical doctor procedures. The forward, inverse kinematics and joint position trajectory equations of the said manipulator also need to be derived. A mathematical model of the robotic manipulator needs to be simulated as well. Simulation results need to be verified experimentally in laboratory conditions. The test results are also compared with the theoretical results. The basic input of every robotic manipulator is the target coordinate and target orientation then come the velocity, acceleration, torque, etc. Without target coordinates and target orientation, the solution of inverse kinematics and velocity equations does not exist. Specially acquiring a real-world target for the robotic manipulator from a CT image proves to be a challenge.
The novelty of this research is mentioned as follows.

- The robotic manipulator designed here comprises 9-DOF and has an arc structure that can be mounted on the CT bed. A train carrying rest of the robot and the needle moves on the arc for better dexterity.
- Inverse kinematics solution of the novel arc and train base structure of the robotic manipulator for the CT bed application.
- A novel 9-DOF robotic manipulator with arc and train structure, servo actuators and sensors are fabricated for experimental analysis under laboratory conditions.
- Design development and testing of an automated robotic system for CT image-guided percutaneous tissue retrieval procedure is done in this research.

2. Nomenclature

$l\ =\ Link\ length$
$d\ =\ Joint\ displacement$
$\alpha\ =\ Link\ twist$
$\theta\ =\ Joint\ angle$
$Cn\ =\ cosine\ of\ nth\ joint$
$C23\ =\ cosine\ (\theta2\ +\ \theta3)$
$Sn\ =\ sine\ of\ nth\ joint$
$S23\ =\ sine\ (\theta2\ +\ \theta3)$
$\Omega\ =\ Orientation\ of\ the\ train\ on\ the\ arc$
$W\ =\ Width\ of\ the\ CT\ bed$
$G\ =\ Length\ of\ the\ arc\ on\ which\ the\ train\ is\ allowed\ to\ travel$
$X, Y\ and\ Z\ =\ Real-world\ target\ coordinates\ of\ the\ robotic\ manipulator$
$n\ =\ joint\ number\ of\ the\ robotic\ manipulator$

3. Robotic Manipulator Design

The robotic manipulator designed here has 9-DOF which includes a novel arc design on which other links of the robot move. An arc type design is developed because of the CT machine environment. The arc-type design will make it easier and ergonomic for the robotic manipulator to maneuver when a human is lying on the CT bed. All the other joints are rotary except for the last two joints, which are prismatic. The DH parameters of the robot designed in this research for retrieving tissue sample using CT image guidance is shown in Table 1.

[Table 1]

The length of penetration for the needle in the human body is denoted by d_{10} in the above DH parameter table and it is found based on the CT scan of the patient.

Based on the DH parameters, a simulation model is developed in MATLAB. This simulation model will be used for simulation and other illustration purposes in this research. Figure 1(a) shows the free-body diagram of the robotic manipulator with an arc structure. Figure 1(b) shows the three-dimensional illustration model developed in MATLAB with arbitrary dimensions for illustration.

[Figure 1(a)] [Figure 1(b)].

A standard rotary 3-DOF, rotary 6-DOF, and a novel 9-DOF hybrid robotic manipulator is designed for this research. The kinematic model of all the robotic manipulators is designed in MATLAB. DH parameters of all the robot manipulators are also found out and mentioned in the respective tables. The red items denote the end effector link and the joints, including rotary and prismatic. While the blue items denote the rest of the links of the robotic manipulators.

Based on the simulation model, 3D-CAD model of the robotic manipulator is designed in SOLIDWORKS 2016. The 3D-CAD of the robotic manipulator is also compared with an average human body placed on a CT machine bed. A CT machine model with real world dimensions of General Electric (GE) CT machine is also designed in SOLIDWORKS 2016 for understanding the feasibility of the robotic manipulator in a CT environment. The robotic manipulator model is shown in figure 2(a) and placing the robotic manipulator on the CT bed with a human body is shown in figure 2(b). [Figure 2(a)] [Figure 2(b)]

Fabrication of the robotic manipulator is done using 3D printing techniques with ABS and carbon fiber reinforced ABS material. Dynamixel servo joint actuators with inbuilt position sensors are used for providing motion. The fabricated robotic manipulator is shown in figure 3.

[Figure 3]

Figure 4 shows the robotic manipulator, CT model, CT blade and adjustable target (Cylindrical tube on the knuckle joint) on a table in laboratory ready for experimentation. All the electronics and power sources are connected as shown in figure 4. This setup is made to simulate the CT machine conditions in a laboratory environment CT bore is 70 cm and CT bed is 40 cm.

[Figure 4]

Once the DH parameters are decided, forward, inverse kinematic and joint position trajectory equations are derived for theoretical simulation.

4. Mathematical formulation

Transformation matrix method is used to formulate the forward kinematics equations. X,Y and Z represent the real world coordinated regarding the base of the robotic manipulator. Equation 1 shows the transformation matrix. Forward kinematic equations of the novel 9-DOF robotic manipulator is shown in equations from 2 to 4.

$$T_{(n-1)}^n = \begin{bmatrix} cos(\theta_n) & -sin(\theta_n) \times cos(\alpha_n) & sin(\theta_n) \times sin(\alpha_n) & l_n \times cos(\theta_n) \\ sin(\theta_n) & cos(\theta_n) \times cos(\alpha_n) & -cos(\theta_n) \times sin(\alpha_n) & l_n \times sin(\theta_n) \\ 0 & sin(\alpha_n) & cos(\alpha_n) & d_n \\ 0 & 0 & 0 & 1 \end{bmatrix} \tag{1}$$

The transformation and orientation equations are shown in equation 2 and 3.

$$T_0^6 = T_0^1 \times T_1^2 \times T_2^3 \times T_3^4 \times T_4^5 \times T_5^6 \times T_6^7 \times T_7^8 \times T_8^9 \times T_9^{10} \tag{2}$$

$$R_0^6 = \begin{bmatrix} n_x & o_x & p_x \\ n_y & o_y & p_y \\ n_z & o_z & p_z \end{bmatrix} \tag{3}$$

Forward kinematic equations of the novel 9-DOF robotic manipulator are shown in equations from 4-6. Here Cn and Sn are cosine and sine of nth joint respectively where, $n = 1, 2 \ldots, n$. $C23$ and $S23$ represent cosine $(\theta_2 + \theta_3)$ and $sine$ $(\theta2 + \theta3)$ and so on respectively.

$$X = l_1 + d_3 + d_8 + d_9 + l_4 * C_7 + l_6 * C_7 - d_5 * S_7 - d_6 * S_7 + l_5 * C_6 * C_7 \tag{4}$$

$$Y = l_3 - l_7 + d_2 - l_8 * C_8 - l_9 * C_8 - l_{10} * C_8 + l_4 * S_7 + l_6 * S_7 + d_5 * C_7 + d_6 * C_7 + d_{10} * S_8 + l_5 * C_6 * S_7 \tag{5}$$

$$Z = l_2 + d_1 + d_4 - d_7 + l_5 * S_6 - l_8 * S_8 - l_9 * S_8 - l_{10} * S_8 - d_{10} * C_8 \tag{6}$$

As the robotic manipulator has 9 DOF, joint constraints are applied so that it can achieve correct orientation while functioning in the CT environment. If the orientation is not as desired, than the needle entry for tissue retrieval cannot be observed by the medical doctors in real time during the CT image acquisition process. The joint constraints are shown by equation 7 to 9. Correct orientation of the end needle is shown in figure 5.

[Figure 5]

$$\theta_3 = 0 \tag{7}$$

$$\theta_4 = \theta_7 \tag{8}$$

$\theta_5 = -\theta_6$ (9)

The train that moves over the arc covers two directions simultaneously $d1$ and $d2$ (Z-axis and Y-axis respectively). As the train moves, there is also a rotation about the X-axis denoted by 'Ω'. All these parameters are interdependent and change according to the travel of the train connected to the rest of the robotic manipulator. The major challenge lies in deriving the equation that connects all the three interdependent motions. The motion of the train depends on the target coordinate in Y-axis. Dimension measured along the CT bed horizontally is Y-axis. The dimension measured vertical to the CT bed is Z-axis. The dimension perpendicular to the frame shown in figure 5 is X-axis. Figure 6 shows the train at a random position on the arc.

[Figure 6]

In figure 6 'S' represents Ψ, the angle between the bed and the leftmost reference line. 'E' represents ε, the angle between the leftmost reference line and the reference line that connects the center of the arc with the train at a random position. 'P' represents Φ the angle of effective operation on the arc, in other terms the angle between the leftmost and rightmost reference line. G represents the length of the arc. W represents the effective width of operation along the Y-axis of the CT bed. 'R' denotes the radius of the arc. Line 'AB' represents 'h', the horizontal distance between the leftmost reference line to the reference line of the train at a random position. Now the equations that interconnect $d1, d2$ and Ω is shown by equation 10 to 21.

$G = R\Phi$ (10)

$\varepsilon = (\Phi Y)/W$ (11)

$h = (YR\Phi)/W = R\varepsilon$ (12)

When, $h > G/2$

$d_1 = R\sin(\pi - (\varepsilon + \psi))$ (13)

$d_2 = R\cos(\pi - (\varepsilon + \psi)) + R$ (14)

$\Omega = \varepsilon - \phi/2$ (15)

When, $h < G/2$

$d_1 = R\sin(\varepsilon + \psi)$ (16)

$d_2 = R - R\cos(\varepsilon + \psi)$ (17)

$\Omega = (\phi/2) - \varepsilon$ (18)

When, $h = G/2$ and

$d_1 = R$

$d_2 = R$

$\Omega = 0$

Now the inverse kinematics of other joints are derived and shown in the equations 19 to 20 for orientations of the joints.

$\theta_6 = \sin^{(-1)}(\frac{((Z-(l_2+d_1+d_4-d_7-l_8*\sin(\theta_8)-l_9*\sin(\theta_8)-l_{10}*\sin(\theta_8)-d_{10}*\cos(\theta_8))))}{l_5})$ (19)

$\theta_7 = \sin^{(-1)}(\frac{((Y-(l_3-l_7+d_2-l_8*\cos(\theta_8)-l_9*\cos(\theta_8)-l_{10}*\cos(\theta_8)+d_{10}*\sin(\theta_8)))}{((l_4+l_6+l_5*\cos(\theta_6)))})$ (20)

Where $\theta_8 = Angle$ $of P enetration$

And $d_{10} = Amount$ of $Penetration$

5

There are multiple ways to generate a trajectory for a robotic manipulator using the joint space method. Linear polynomial equations can generate a trajectory for the actuator. The cubic polynomial is one such polynomial. It is also very easy and computationally inexpensive to solve. However, the downside of this method is that the first derivative of the cubic polynomial is discontinuous at the beginning and the end. This property makes the velocity of the actuator discontinuous at the start and the end of the trajectory. Hence, the path tracing becomes jittery at the beginning and the end, causing a lot of vibration. To rectify this problem of discontinuity, implementing parabolic blends are made at the beginning and the end of the trajectory. Parabolic blends refer to acceleration while starting the actuator and deceleration at the end. Figure 7 shows the desired 'S' curve profile and equations 21 to 23 shows the joint trajectory equations necessary for generating this profile.

[Figure 7]

$$\theta_p = \theta_0 - 0.5tt_b{}^2\ddot{\theta} + \ddot{\theta}tt_bt_p \tag{21}$$

$$\theta_p = \theta_0 - 0.5t_p{}^2\ddot{\theta} \tag{22}$$

$$\theta_p = \theta_f - 0.5(t_f - t_p)^2\ddot{\theta} \tag{23}$$

To form a complete parabolic trajectory for an actuator, equations 21, 22 and 23 are set up in a specific sequence of time history. Equation 24 is used until time t_b then equation 22 is used from time $tb\ to\ tf - tb$. After equation 22, equation 23 is used from time $tf - tb\ to\ tf$ as shown in figure 7.

5. Theoretical Simulation and Experimentation

MATLAB is used for the mathematical simulation of the robotic manipulator. A set of target coordinates is taken for a CT image using CT machine software, as shown in figure 8. This target point is used for simulation and experimentation purposes as well.

[Figure 8]

Target acquired for the robotic manipulator using the CT image with the help of an expert radiologist from KIMS hospital, Bhubaneswar is shown in the table 2 below.

[Table 2]

Figure 9 shows the simulation model and the experimental model side by side at the home position. It is observed that the experimental model with a biopsy needle attached to its end closely resembles the simulation model.

[Figure 9]

To test the deviation analysis of the robotic manipulator prototype, two camera image acquisition and processing setup is implemented. A basler ACA smart camera acquires front view images and a Logitech camera captures the top view. Pixel distance is then converted to real-world coordinates to get the accurate deviation results. Using this setup target is also set for the robotic manipulator in the laboratory. Figure 10(a) shows the targets in the experimental environment and Figure 10(b) shows the target in the theoretical simulation environment.

[Figure 10(a)] [Figure 10(b)]

The Robotic manipulator is now programmed to reach the target point and insert the needle into the target up to a desired depth. Image processing setup acquires the deviation data from the front view and the top view as shown in figure 11(a). The experiment is performed 5 times at this target point to check the repeatability of the robotic manipulator. Figure 11(b) shows the theoretical simulation model at the target point as well.

[Figure 11(a)][Figure 11(b)]

6. Results and Discussion

After the experimentation is completed, the results of the overall and joint deviations is found and the reasons for the deviation are discussed. Table 3 shows the comparison of input target parameters and output target positions found using image processing setup.

[Table 3]

From the above table it is observed that the deviation does not exceed 0.3 cm or 3 mm for the target position on X-axis and the deviation does not exceed 0.32 cm or 3.2 mm in the positive direction and 0.15 cm or 1.5 mm in the negative direction for the target position in Y-axis. It is also observed that the deviation does not exceed 0.28 cm or 2.8 mm in the positive direction and 0.14 cm or 1.4 mm in the negative direction for the target positions in Z-axis. The deviation of the needle insertion does not exceed 0.05 cm or 0.5 mm in the positive direction and 0.15 cm or 1.5 mm in the negative direction. These deviations are within acceptable parameters. The deviation in needle placement should not exceed 5mm in each direction, according to the expert radiologists in KIMS Hospital, Bhubaneswar.

As observed in table 6.6, there deviates from the desired first and second target position for targets 1-4, respectively. Some reasons for deviation are apparent from the analysis of the experimental images. The reason for the deviation is the tolerance of the actuators. The dynamical servo actuators used in the fabrication of the robotic manipulator are $\pm 0.29°$. Deviation in reaching the target position will occur if an actuator overshoots or undershoots by $0.29°$. Some deviation is found in reaching the desired joint position of the servo actuator when the torque requirement for the servo actuator increases. As this is only an experimental model of the robotic manipulator, there is a little undesired motion between the parts of the 3D printed linear actuators. This also causes a slight deviation in reaching the first target position and the second target position. To understand the reasons for deviation, trajectory analysis of each servo actuator is performed using the position data from the servo actuators.

Initially, the train moves on the arc, according to the trajectory followed by the robotic manipulator. Prismatic distance d_2 is measured using the ultrasonic distance sensor placed for control of the position of the train on the arc. The real-time distance is measured for all the targets. In all the graphs, the red dotted line shows the ideal trajectory while the blue line shows the trajectory of the train for experiment 1 of target. Green-line shows the trajectory of the train for experiment 2 of target. The yellow line shows the trajectory of the train for experiment 3 of target. Black-line shows the trajectory of the train for experiment 4 of target. The magenta line shows the trajectory of the train for experiment 5 of target. Figure 12 shows the comparison graph of theoretical and experimental joint trajectory profiles of all the joints.

[Figure 12. (a), (b). (c), (d), (e), (f), (g), (h)]

Five experiments for the target point are conducted to visualize the repeatability of the robotic manipulator. Evaluation of deviation in reaching the target positions for all the experiments revealed it does not exceed 5 mm in X, Y or Z direction. In most cases, the deviation lies between 0.1 to 3.8 mm in each of the three X, Y, or Z directions. The deviation in the angle of insertion is also within $1°$. In most cases, the angle of deviation lies between $0.4°$ to $0.55°$. To understand the reasons for the deviation and analyze the positional trajectory profile, real-time actuator sensor data is plotted with respect to the theoretical curve. It is observed that there is a slight deviation in following the theoretical position trajectory. However, the profile of the positional trajectory follows a smooth continuous 'S' curve, and this proves that the joint motion has minimal vibrations while functioning. The joint trajectory follows the desired 'S' curve profile in most cases, where torque requirement is low. Deviations in following the desired profile are higher where torque requirement is high and the difference between the home position and target joint position is less. The desired joint position is reached smoothly.

A comparison table of the average deviation analysis is shown with the existing robotic system developed by Maarten Menno Arnolli, Perfint MAXIO, Amedo LNS and the robotic manipulator developed in this research. It is observed that all the robotic manipulators except Perfint MAXIO are ≤ 5 mm allowable error limit. The deviation of the robotic manipulator developed in this research is comparable to other systems and better in some cases which is shown in Table 4.

[Table 4]

7. Conclusion

In this research, a robotic manipulator is designed, fabricated and tested to retrieve abnormal tissue under CT image guidance. The robotic manipulator has 9 DOF and an arc and train structure. 9-DOF manipulator helps in the needle's manipulation with more versatility in the CT environment. DH parameters for the such novel robotic manipulator is formulated. Forward and inverse kinematics equations helped in obtaining the joint angles required to reach the desired target. Inverse kinematics derived for the arc design yielded accurate results evident in the theoretical simulation. The simulation achieved a smooth and continuous motion with a slow start and a slow stop for reduced vibration and jerk. This was accomplished with the use of symmetric parabolic blends at the beginning and the end of a linear profile, a.k.a. 'S' curve. The experimental prototype of the robotic manipulator validates the theoretical part. CT environment is simulated in laboratory conditions for experimentations. The performance of the trained AI model LiverNet3.0 is compared with expert radiologists at KIMS hospital, Bhubaneswar in a case series of 50 patients to understand its accuracy in the medical environment. LiverNet3.0 provided satisfactory results with an accuracy of 92% and a Kappa score of 92.94%. Although the accuracy and the kappa score is a little less as compared to the accuracy of the radiologists the results were promising. The abnormal lesions are located in the CT image using the novel AI system with the help of a box surrounding them. The middle point of these boxes is considered as the final or second target point for the robotic manipulator. An expert radiologist advised on the correct path of needle insertion including the first target point and angle of insertion for four patients with lesions at different locations of the liver. Target is acquired from the CT image with the help of an expert radiologist. From the results of the experiment, it is concluded that the deviation of the robotic manipulator is within acceptable limits of 5 mm in needle placement and 1° in needle orientation. All the joints with dynamixel servo actuator followed the 'S' curve profile but the joints requiring high torque deviated slightly from the trajectory but they reached the target position. This could be rectified by using actuators with high torque capacity.

In conclusion, it can be said that the experimental model of the robotic manipulator performed successfully in laboratory conditions without colliding with the CT model. The deviations were also within the tolerance limits and the reasons for these deviations are discussed.

References

[1] Shubham Kamlesh, S., and Mishra, R. "Advanced path simulation of a 5R robotic arm for CT guided medical procedures", Materials Today: Proceedings, 5(2), 6149-6156 (2018).

[2] Shah, S., Mishra, R., and Choudhury, S. "Preliminary design of an 7 DOF robotic manipulator positioning biopsy needle", Materials Today: Proceedings, 5(9), 19140-19146 (2018).

[3] Shah, S., Mishra, R., Mishra, B., and Pandey, O. "Prediction of abnormal hepatic region using ROI thresholding-based segmentation and deep learning-based classification", International Journal Of Computer Applications In Technology, 64(4), 382 (2020).

[4] Shah, S., Mishra, R., Szczurowska, A., and Guziński, M. "Non-invasive multi-channel deep learning convolutional neural networks for localization and classification of common hepatic lesions", Polish Journal of Radiology, 86, e440–e448(2021).

[5] Shah, S., and Mishra, R. "Modelling and Optimization of Robotic Manipulator Mechanism for Computed Tomography Guided Medical Procedure", Scientia Iranica, 29(2 B), pp. 543-555 (2021).

[6] Northern Digital Inc., 103 Randall Drive, Waterloo, Ontario, N2V 1C5, Canada. http://www.ndigital.com.

[7] Claron Technology Inc., 120 Carlton Street, Suite 217, Toronto, Ontario, M5A 4K2, Canada. http://www.clarontech.com.

[8] K.A. Gavaghan, S. Anderegg, M. Peterhans, T. Oliveira-Santos, and S. Weber. "Augmented reality image overlay projection for image guided open liver ablation of metastatic liver cancer", In Augmented Environments for Computer-Assisted Interventions, volume 7264 of Lecture Notes in Computer Science, pages 36–46. 2012.

[9] Pathfinder, 2969 Armory Drive, Suite 100A, Nashville, Tennessee, 37204, USA. http://www.pathnav.com.

[10] Medtronic, 710 Medtronic Parkway, Minneapolis, Minnesota, 55432-5604, USA. http://www.medtronic.com.

[11] Stryker, 2825 Airview Boulevard, Kalamazoo, Michigan, 49002, USA.http://www.stryker.com.

[12] CAScination AG, Stauffacherstrasse 78, 3008 Bern, Switserland.http://www.cascination.com.

[13] ActiViews, Inc., 591 North Avenue, Entry One, Wakefield, Massachusetts,01880, USA. http://www.activiews.com.

[14] P. Gilboa, inventor; Activiews Ltd., assignee, "System and method for optical position measurement and guidance of a rigid or semi-flexible tool toa target", US patent 7,876,942 B2, January 25, 2011.

[15] S.R.H. Barrett, N.C. Hanumara, C.J. Walsh, A.H. Slocum, R. Gupta, and J.O. Shepard. "A remote needle guidance system for percutaneous biopsies", In Proceedings of the ASME 2005 International Design Engineering Technical Conferences and Computers and Information in Engineering Conference (IDETC/CIE), volume 7, pages 481–189, Long Beach, California, USA, 2005.

[16] Royal Philips, Amstelplein 2, Breitner Center, 1096 BC, Amsterdam, theNetherlands. http://www.philips.com.

[17] J.H. Yanof, L.L. Goldstein, F.C. Jensen, J.C. Foster, and C. Bauer, inventors; Picker International Inc., assignee. Interchangeable guidance devices for C.T. assisted surgery and method of using same. US patent 5,957,933, September 28, 1999.

[18] J.H. Yanof, P.H. Klahr, and L. O'Donnell, inventors; Picker InternationalInc., assignee. Frameless stereotactic CT scanner with virtual needle display for planning image guided interventional procedures. US patent6,064,904, May 16, 2000.

[19] J.M. Hevezi, M. Blough, D. Hoffmeyer, and J.H. Yan of." Brachytherapy using CT Pin Point". MEDICAMUNDI, 46(3):22–27, 2002.

[20] Immersion Corporation, 30 Rio Robles, San Jose, California, 95134, USA.http://www.immersion.com

[21] NeoRad AS, Gaustadalléen 21, 0349, Oslo, Norway.http://www.neorad.no.

[22] K. Brabrand, N. Bérard-Andersen, G.F. Olsen, and V. Bakke, inventors; Neo Rad A/S, applicant. Needle holder. US patent application 2012/0022368A1, January 26, 2012.

[23] AprioMed AB, Virdings Allé 28, 754 50, Uppsala, Sweden.http://www.apriomed.com.

[24] A. Magnusson, E. Radecka, M. Lönnemark, and H. Raland. "Computed-tomography-guided punctures using a new guidance device", ActaRadiologica, 46(5):505–509, 2005.

[25] R. Gupta, S.R.H. Barrett, N.C. Hanumara, J.O. Shepard, A.H. Slocum, andC.J. Walsh, inventors. "Guidance and insertion system". US patent application 2006/0229641 A1, October 12, 2006.

[26] Bard International, Inc., 730 Central Avenue, Murray Hill, New Jersey,07974, USA. http://www.crbard.com.

[27] A. Magnusson, and D. Åkerfeldt, inventors; Bard International, Inc., assignee. "Puncture guide for computer tomography". US patent 5,280,427, January 18, 1994.

[28] A. Magnusson and D. Åkerfeldt. CT-guided core biopsy using a new guidance device. ActaRadiologica, 32(1):83–85, 1991.

[29] D. Stoianovici, D. Mazilu, and L.R. Kavoussi, inventors; The Johns HopkinsUniversity, assignee. "Robot for computed tomography interventions",US patent 7,822,466 B2, October 26, 2010.

[30] D. Stoianovici, K. Cleary, A. Patriciu, D. Mazilu, A. Stanimir, N. Craciunoiu,V. Watson, and L. Kavoussi. "AcuBot: a robot for radiological interventions", IEEE Transactions on Robotics and Automation, 19(5):927–930, 2003.

[31] Arnolli, M., Buijze, M., Franken, M., de Jong, K., Brouwer, D. and Broeders, I., "System for CT-guided needle placement in the thorax and abdomen: A design for clinical acceptability, applicability and usability", The International Journal of Medical Robotics and Computer Assisted Surgery, 14(1), p.e1877 (2017

[32] Kumari, K. S., Samal, S., Mishra, R., Madiraju, G., Mahabob, M. N., and Shivappa, A. B. "Diagnosing COVID-19 from CT image of lung segmentation & classification with deep learning based on convolutional neural networks", Wireless Personal Communications, doi:10.1007/s11277-021-09076-w (2021).

[33] Shah, S., Mishra, R., Pramanik, S., Kundu, A., Pandit, S., and Mallick, A. "*Design and deviation analysis of a semi-automated needle manipulation system using image processing technique*",1045, pp. 279-288 (2020).

[34] Fahim, S. Sarker, Y. and Sarker, S. "Modeling and development of a five DoF vision based remote operated robotic arm with transmission control protocol", SN Applied Sciences, vol. 2, no. 7 (2020).

[35] Korayem, M., and Yousefzadeh, M. "Adaptive control of a cable-actuated parallel manipulator mounted on a platform with differential wheels under payload uncertainty", *Scientia Iranica*, 27(1), 273-286(2020).

[36] Wu, J., Wang, X., Zhang, B., and Huang, T. "Multi-objective optimal design of a novel 6-DOF spray-painting robot". Robotica, 39(12), 2268-2282 (2021).

[37] Wu, J., Zhang, B., Wang, L. *et al.* "An iterative learning method for realizing accurate dynamic feedforward control of an industrial hybrid robot". *Sci. China Technol. Sci.* 64, 1177–1188 (2021).

[38] Jun Wu, Jinsong Wang, Zheng You, "An overview of dynamic parameter identification of robots", Robotics and Computer-Integrated Manufacturing, Volume 26, Issue 5, Pages 414-419 (2010).

[39] T. Gruber-Rouh, C. Lee, J. Bolck, N.N.N. Naguib, *et al.* "Intervention planning using a laser navigation system for CT-guided interventions: a phantom and patient study". Korean journal of radiology, 16(4):729—735, 2015.

[40] Y. Koethe, S. Xu, G. Velusamy, B.J. Wood, and A.M. Venkatesan. "Accuracy and efficacy of percutaneous biopsy and ablation using robotic assistance under computed tomography guidance a phantom study", European Radiology, 24(3):723–730, 2014.

[41] Arnolli, M., Buijze, M., Franken, M., de Jong, K., Brouwer, D. and Broeders, I., "System for CT-guided needle placement in the thorax and abdomen: A design for clinical acceptability, applicability and usability",The International Journal of Medical Robotics and Computer Assisted Surgery, 14(1) 2017, p.e1877.

Technical Bibliography

1. **Shubham Kamlesh Shah**

   Shubham Kamlesh Shah is a PhD research scholar at School of Mechanical Engineering, KIIT deemed to be University. He specialized in robotics, machine learning and machine design. He completed his Bachelors in technology and Masters in technology in Mechanical engineering and machine design from KIIT Deemed to be University, Bhubaneswar, Odisha India. He has published many research articles in international journal and conferences. He also has three national and international patents published.

2. **Ruby Mishra***

   Ruby Mishra* received B.E (Mechanical Engineering) from Utkal University in 1999, MTech (Machine Design) from Jadavpur University, in 2007, and Ph.D. (Machine Design) from Jadavpur University in 2014. She has a teaching and research experience of 22 years. Her research interests include Kinematics of Machine and Mechanism, Biomedical Engineering, Biomedical signal and image processing, robotics, medical image analysis. She is a member of The Institute of Engineers and Indian Science Congress Association. She has published four national and international patents. She

has published many articles that are indexed in Scopus, Web of Science, and Google Scholar. Currently, she is doing research on Biomedical Instruments like Robotic arm for C.T. Guided Biopsy and Single Lumen Micro catheter for Angiography and Embolization. At present, she is working as an Associate Professor in the School of Mechanical Engineering Department of KIIT Deemed to be University.

Appendices sections:

List of Figures

SL. No.	Figure No.	Figure Caption
1	Figure 1(a)	Free body diagram of a 9-DOF robotic manipulator
2	Figure 1(b)	Simulation model of 9-DOF robotic manipulator developed in MATLAB
3	Figure 2 (a)	Isometric view of the fully assembled robotic manipulator CAD model.
4	Figure 2 (b)	Isometric view of the fully assembled robotic manipulator with CT machine CAD model.
5	Figure 3	Experimental prototype of the robotic manipulator.
6	Figure 4	Complete experimental model of the robotic manipulator
7	Figure 5	Correct orientation of the robot manipulator ready for needle penetration
8	Figure 6	Train is at a random position on the arc.
9	Figure 7	Complete parabolic blend trajectory.
10	Figure 8	Target acquisition for the robotic manipulator from CT image
11	Figure 9	Experimentation model and simulation model of the robotic manipulator at home position.
12	Figure 10(a)	Target setup in laboratory environment.
13	Figure 10(b)	Target setup in theoretical simulation environment
14	Figure 11(a)	Deviation analysis of the robotic manipulator at the target.
15	Figure 11(b)	Simulation model of the robotic manipulator at the target
16	Figure 12(a), (b). (c), (d), (e), (f), (g), (h)	Theoretical and experimental joint trajectory profiles of $d2, \theta3, \theta4, \theta5, \theta6, \theta7, \theta8$ and $d9$.

List of Tables

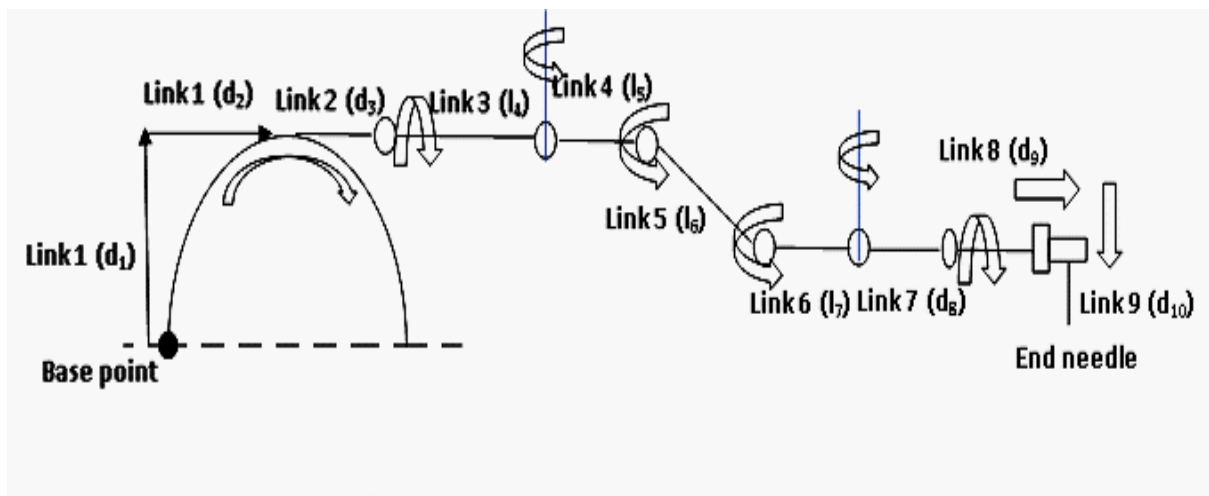| SL. No.	Table No.	Table Caption
1	Table 1	DH parameters of the 9-DOF robot manipulator.
2	Table 2	Targets acquired for the robotic manipulator from the CT Image
3	Table 3	Comparison of input and output target.
4	Table 4	Comparison of deviation analysis of the robotic manipulator.

Figures

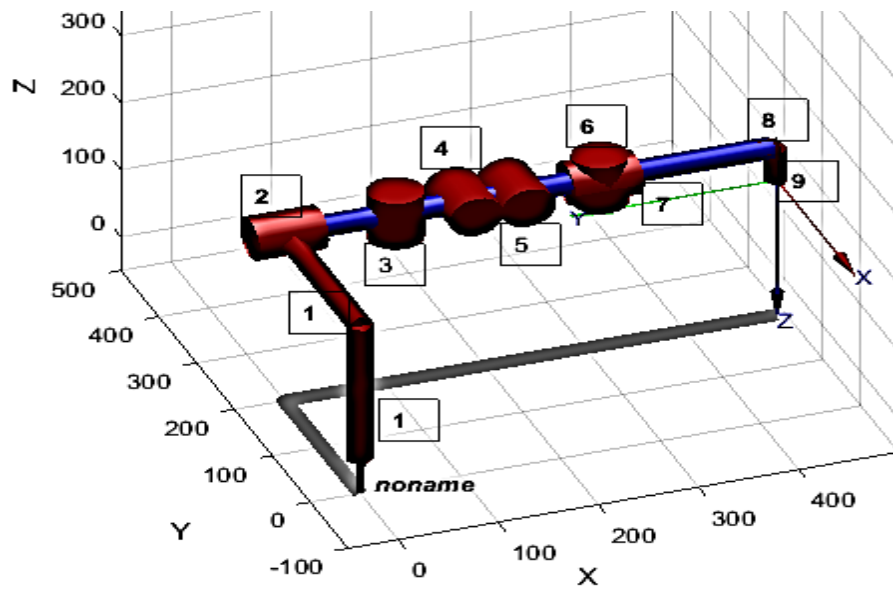Fig. 1(a) Free-body diagram of a 9-DOF robotic manipulator.

Fig.1(b) Simulation model of 9-DOF robotic manipulator developed in MATLAB.
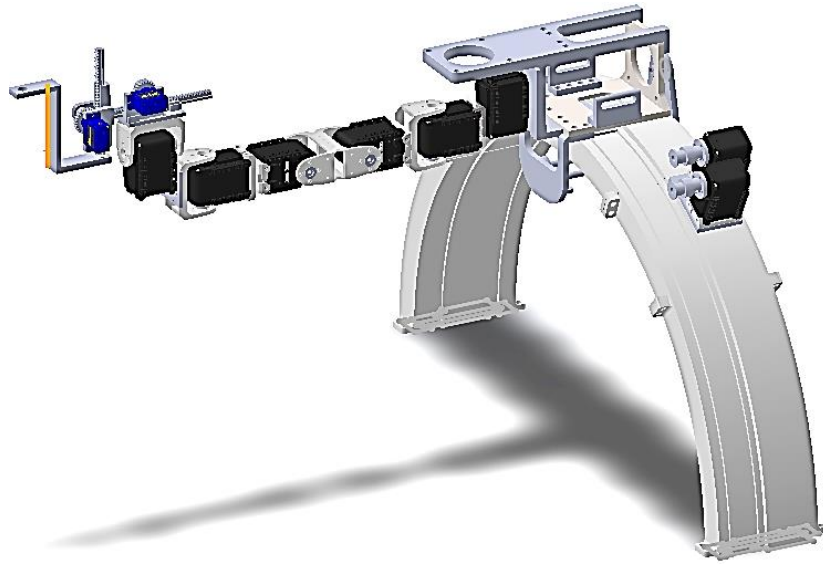
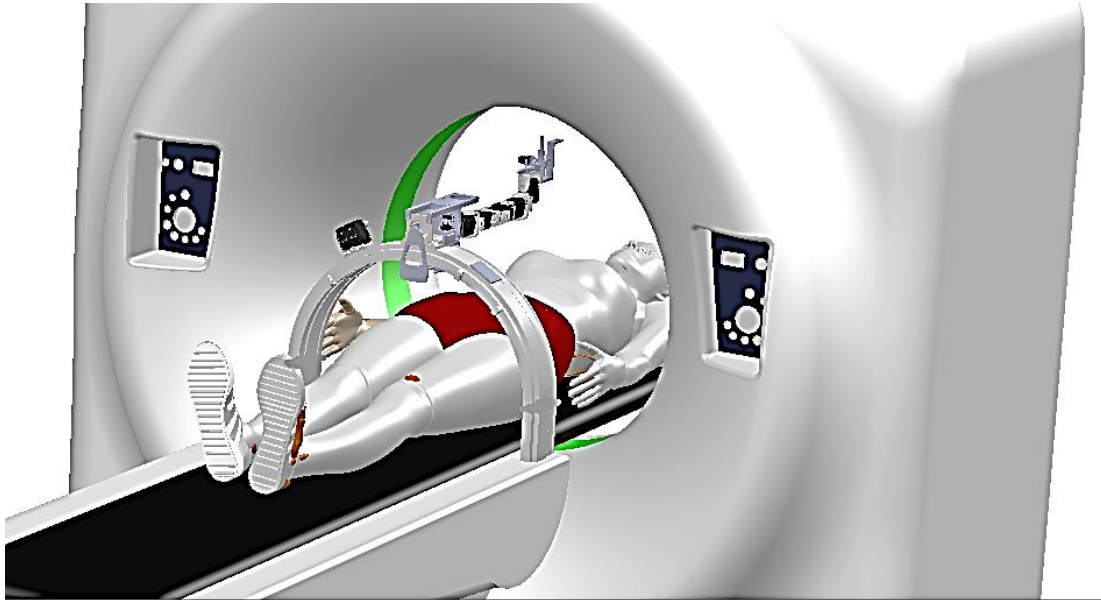Fig.2(a) Isometric view of the fully assembled robotic manipulator CAD model

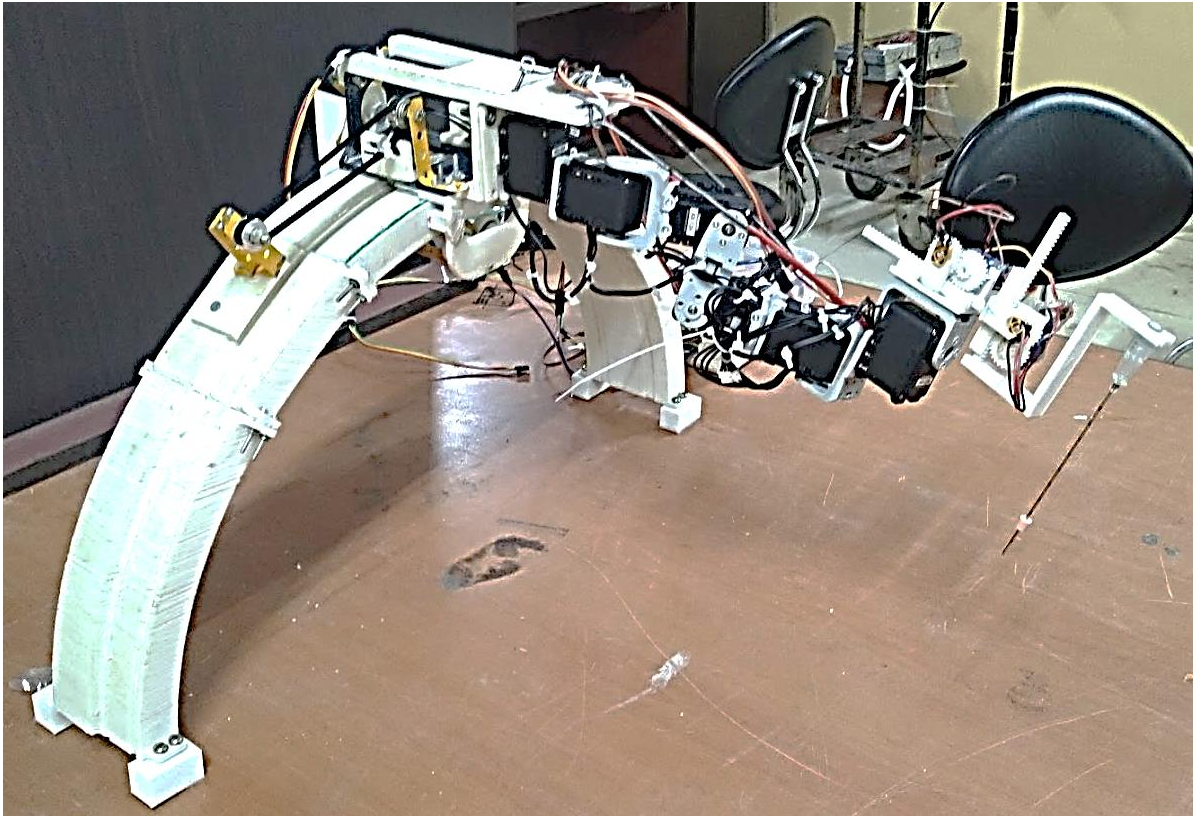Fig. 2(b) Isometric view of the fully assembled robotic manipulator with CT machine CAD model.

Fig. 3 Experimental prototype of the robotic manipulator.

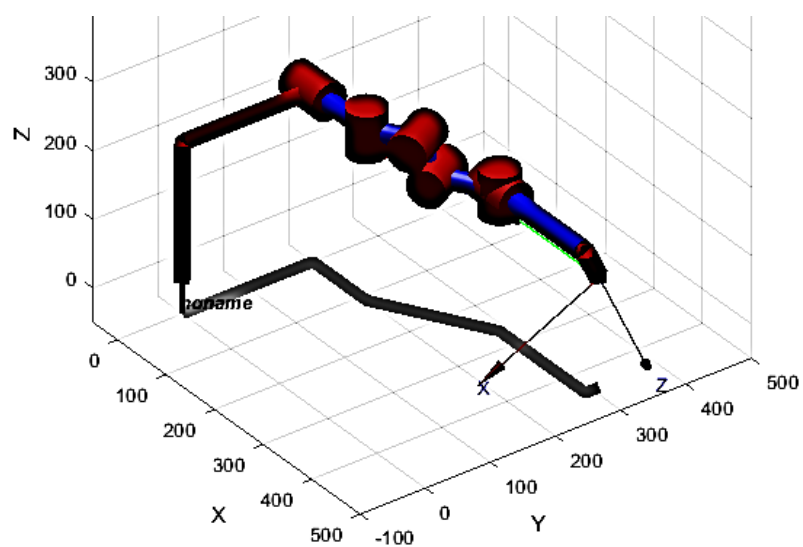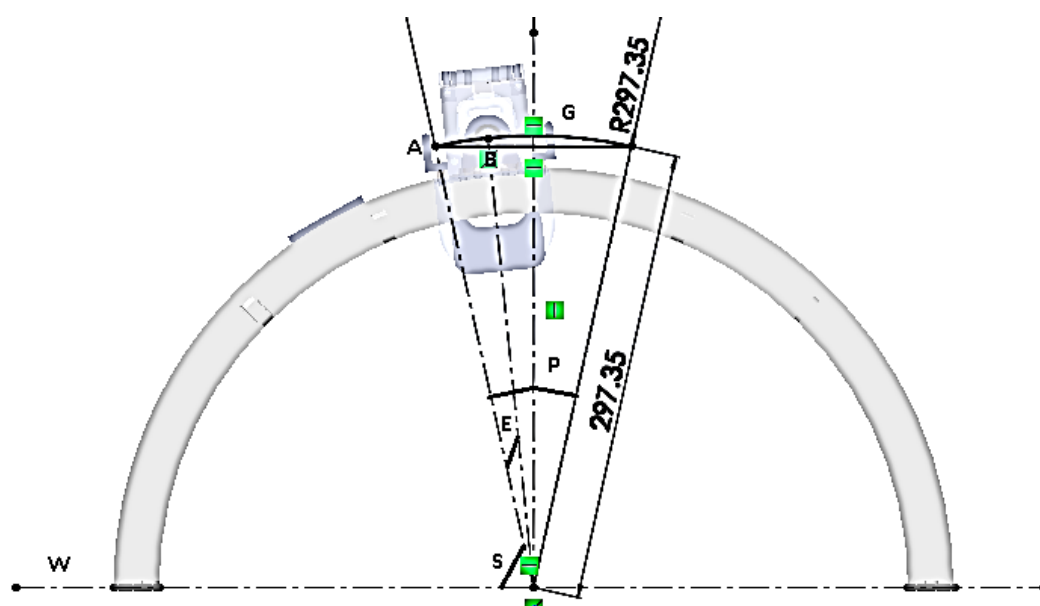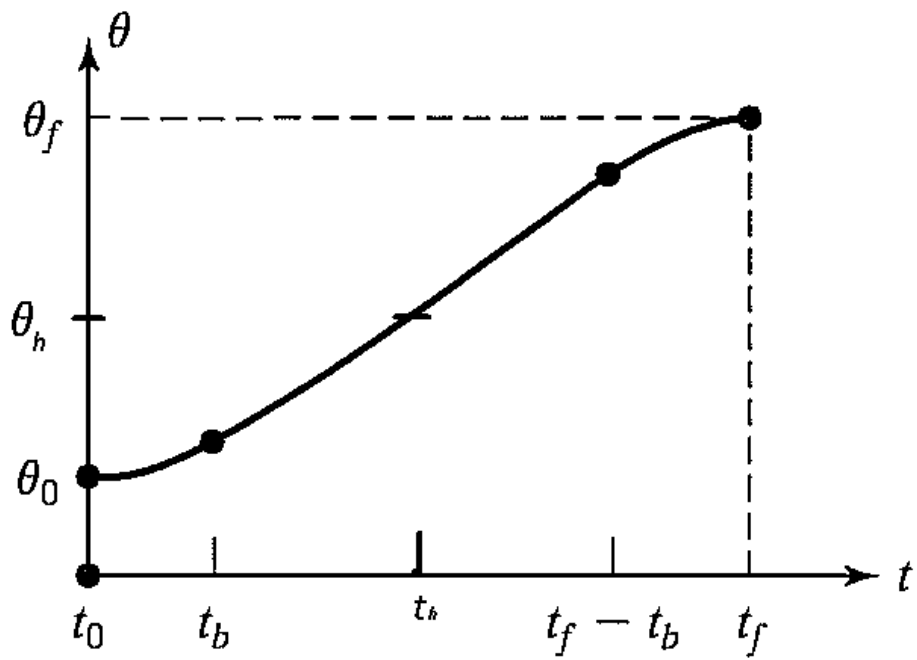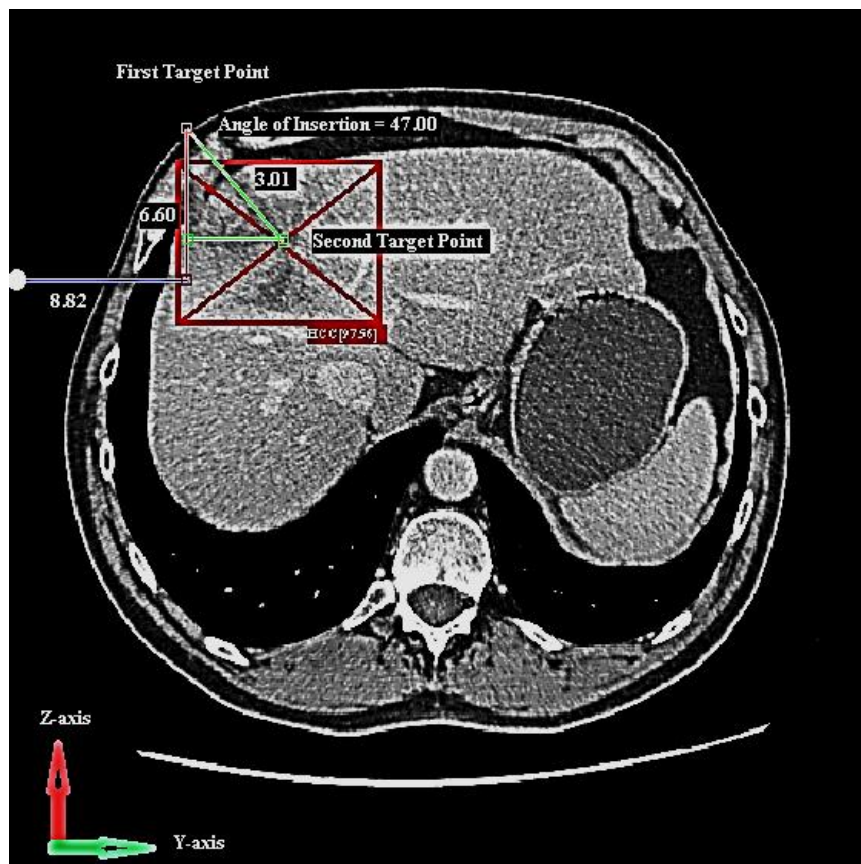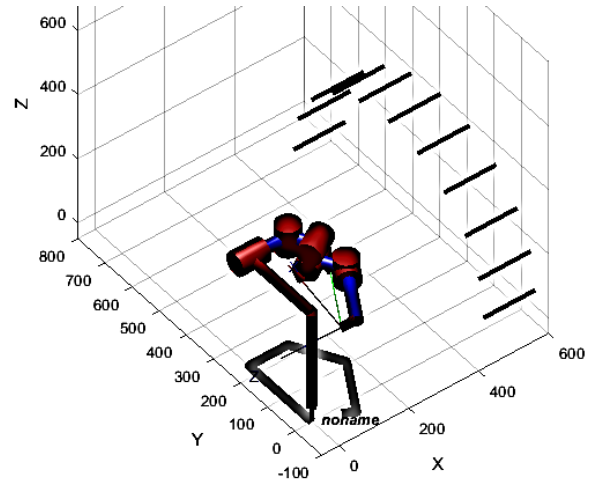Fig. 4 Complete experimental model of the robotic manipulator.

Fig. 5. Correct orientation of the robot manipulator ready for needle penetration.

Fig. 6 Train is at a random position on the arc.

Fig. 7 Complete parabolic blend trajectory.

Fig. 8 Target acquisition of the robotic manipulator from CT image.

Fig. 9 Experimentation model and simulation model of the robotic manipulator at home position.
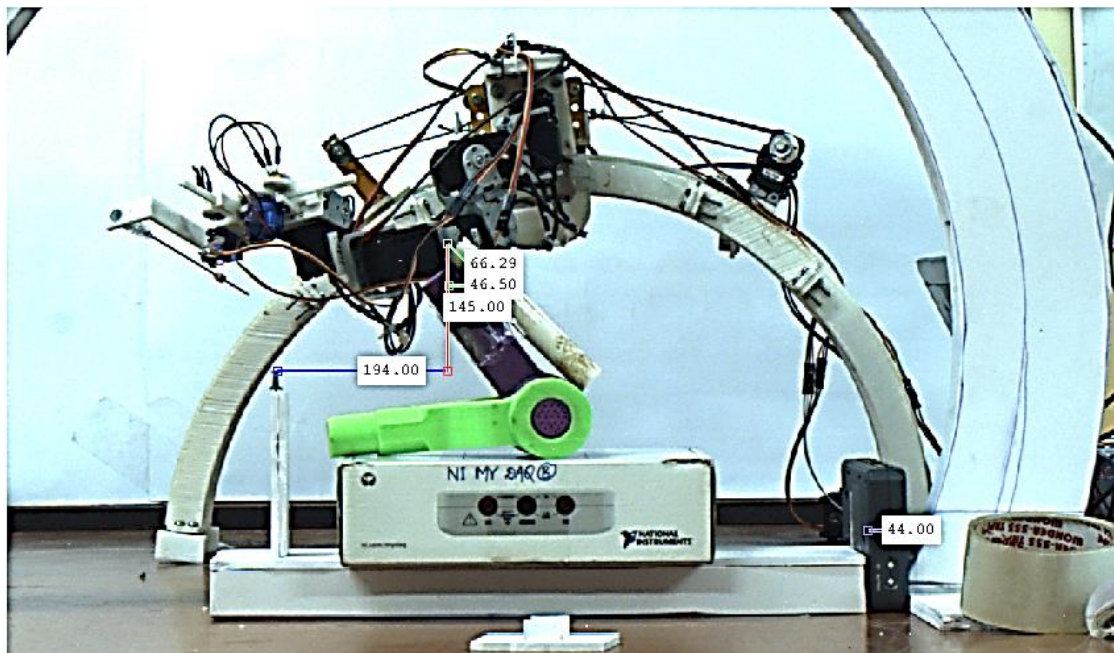
Fig. 10(a) Target setup in the laboratory environment.
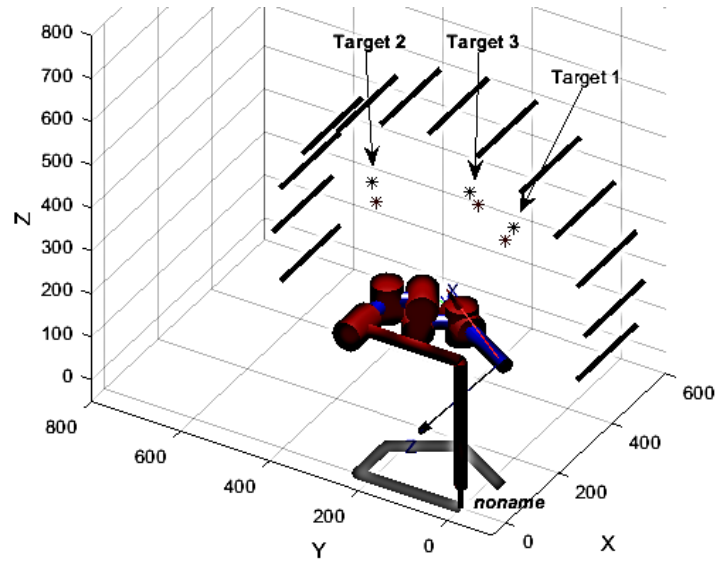
Fig. 10(b) Target setup in the theoretical simulation environment.

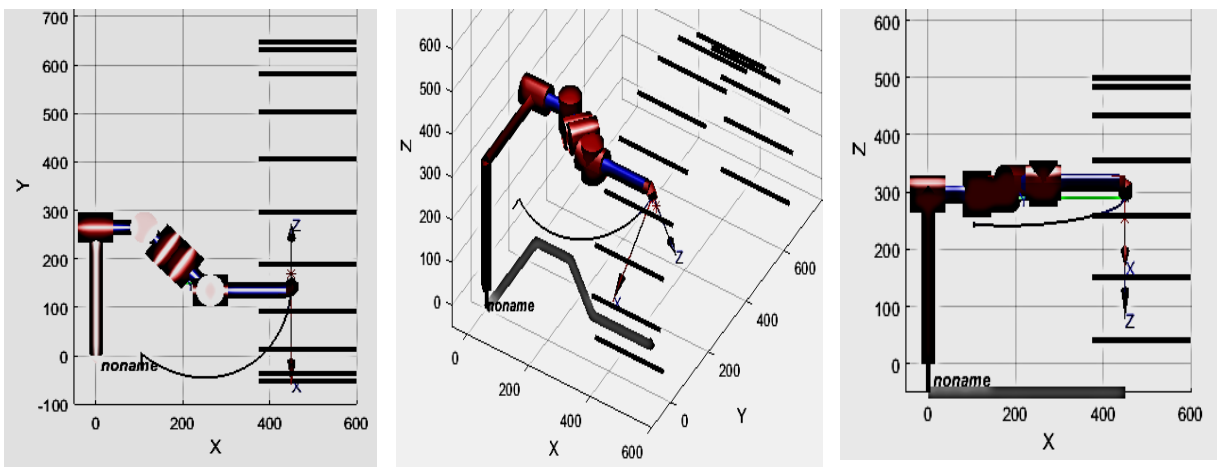Fig. 11(a) Deviation analysis of the robotic manipulator at the target.

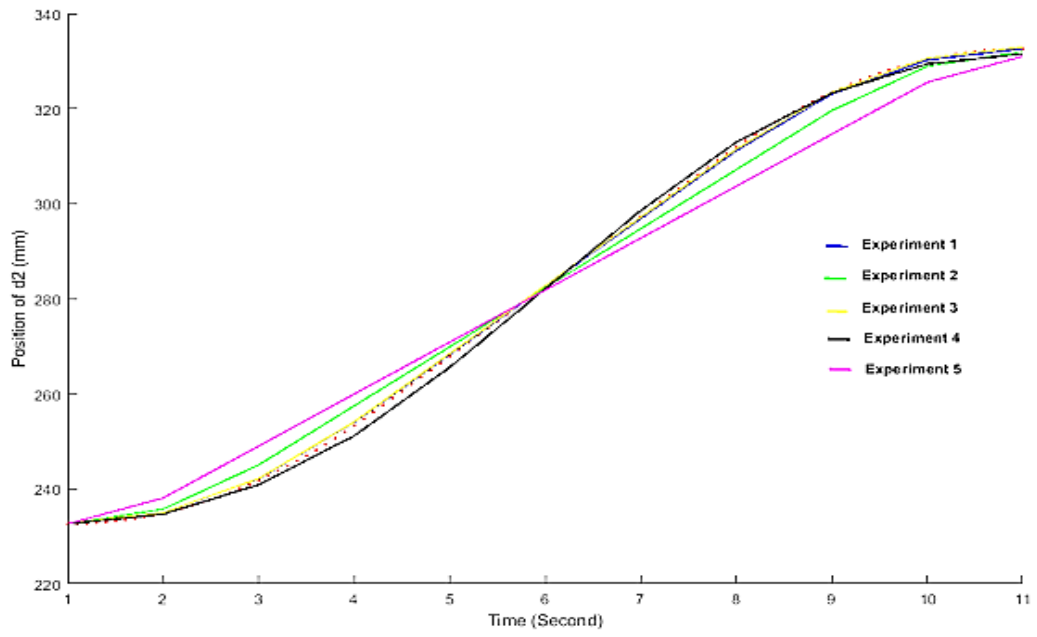Fig. 11(b) Simulation model of the robotic manipulator at the target.

Fig. 12(a)Theoretical and experimental joint trajectory profiles of d_2
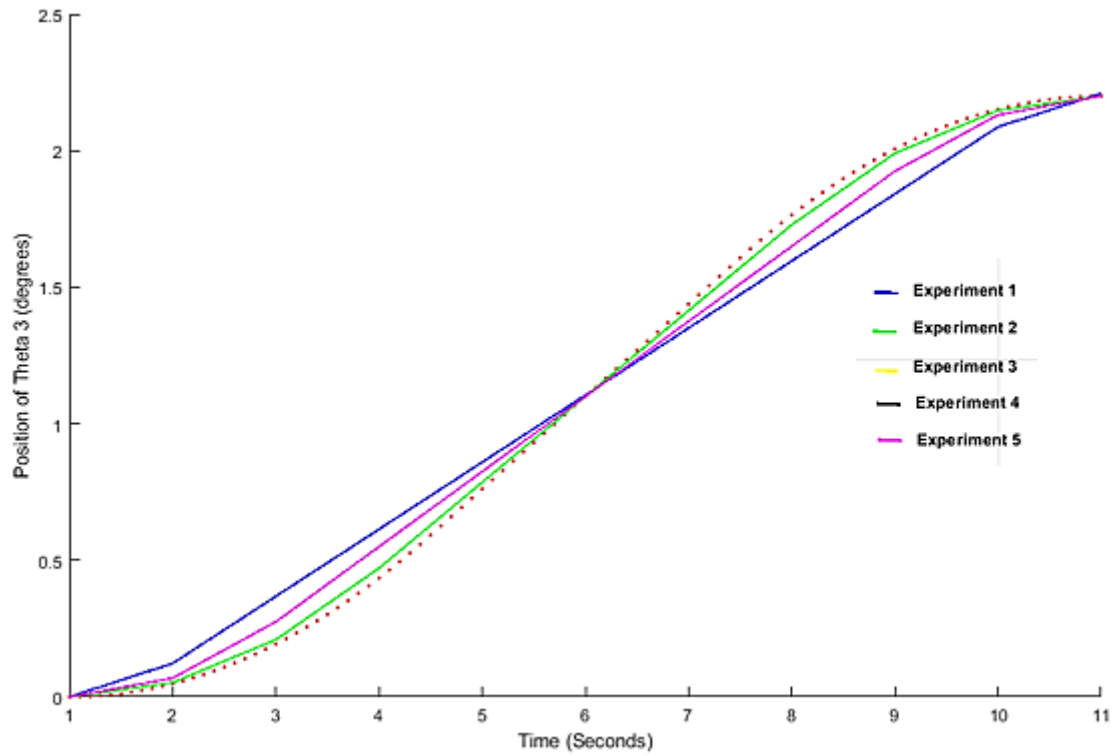

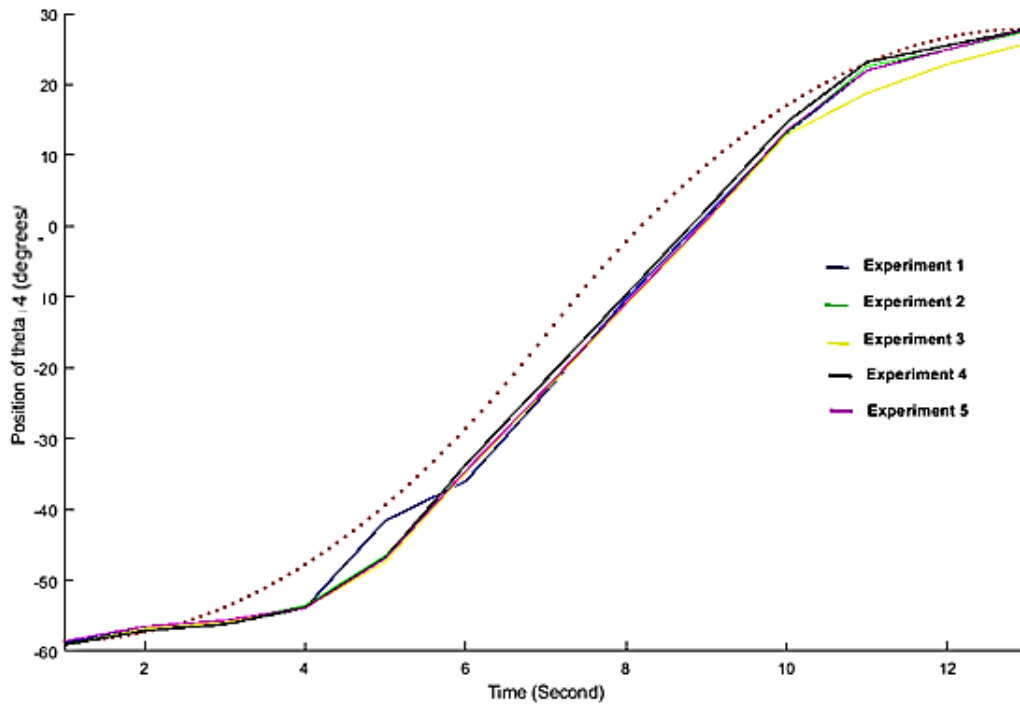Fig.12(b). Theoretical and experimental joint trajectory profiles of θ_3

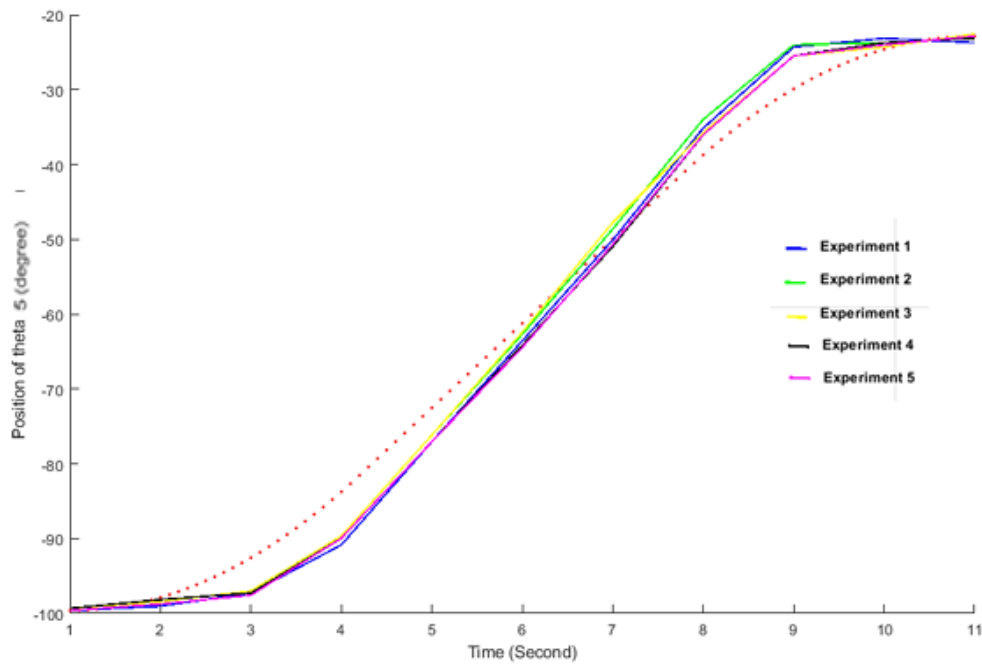Fig.12(c). Theoretical and experimental joint trajectory profiles of θ_4.

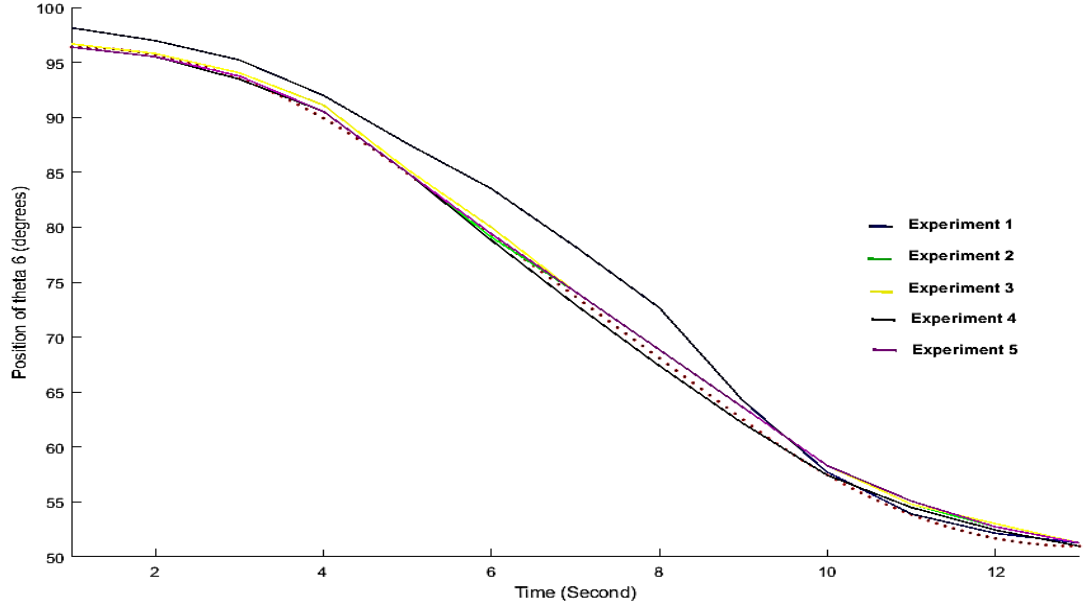Fig.12(d). Theoretical and experimental joint trajectory profiles of θ_5

Fig.12(e). Theoretical and experimental joint trajectory profiles of θ_6.

Tables

Table 1. DH parameters of the 9-DOF robot manipulator.

Link Number	Link length (li)	Joint Displacement (di)	Link Twist (αi)	Joint Angle (θi)
Link 1	$l1$	$d1 = 40cm$	$-\pi/2$	0
Link 1	$l2$	$d2 = 20cm$	$-\pi/2$	$-\pi/2$
Link 2	0	$d3 = 1.02cm$	$-\pi/2$	$\theta3 - \pi/2$
Link 3	$l4 = 9.9cm$	0	$-\pi/2$	$\theta4 - \pi/2$
Link 4	$l5 = 19.9cm$	0	0	$\theta5$
Link 5	$l6 = 10.7cm$	0	$-\pi/2$	$\theta6$
Link 6	0	0	$\pi/2$	$\theta7 + \pi/2$
Link 7	0	$d8 = 2.9cm$	0	$\theta8$
Link 8	0	$d9 = 4.9cm$	0	0
Link 9	0	$d10$	0	0

Table 2. Targets acquired for the robotic manipulator from the CT Image

	X coordinate (cm)	Y coordinate (cm)	Z coordinate (cm)	Amount of insertion	Angle of insertion
Target 1	50	8.82	6.6	3.01	47 .00°

Table 3. Comparison of input and output target.

Sr. No	Input target in cm				Input Angle of insertion	Output target in cm				Output Angle of insertion
	X''	Y''	Z''	Amount of insertion		X''	Y''	Z''	Amount of insertion	
1	0	8.82	6.6	3.01	47 .00°	0.133	8.750	6.509	2.988	47.22°
2	0	8.82	6.6	3.01	47 .00°	0.134	8.793	6.671	3.023	46.50°
3	0	8.82	6.6	3.01	47 .00°	0.142	8.894	6.499	3.043	46.12°
4	0	8.82	6.6	3.01	47 .00°	0.126	8.784	6.690	2.992	47.13°
5	0	8.82	6.6	3.01	47 .00°	0.123	8.780	6.559	3.016	46.64°

Table 4. Comparison of deviation analysis of the robotic manipulator.

Deviation in	Maarten Menno Arnolli [41]	Perfint MAXIO [40]	Amedo LNS [39]	Current Research
X axis	2.6 mm	6.8 mm	2.9 mm	2.7 mm
Y axis	2.8 mm	7.2 mm	3.7 mm	3.1 mm
Z axis	3.3 mm	4.9 mm	4.8 mm	2.7 mm
Depth of Insertion	1.27 mm	6.5 mm	4.0 mm	1.51 mm